Theoretical Studies of the Reaction Mechanisms of Dimethylsulfide and Dimethylselenide with Peroxynitrite

Djamaladdin G. Musaev*

Cherry L. Emerson Center for Scientific Computation, Emory University, 1515 Pierce Drive, Atlanta, Georgia 30322

Yurii V. Geletii and Craig L. Hill

Department of Chemistry, Emory University, 1515 Pierce Drive, Atlanta, Georgia 30322

Received: April 28, 2003; In Final Form: May 22, 2003

The mechanisms of the reactions of dimethylsulfide (DMS) and dimethylselenide (DMSe) with peroxynitrite anion, $ONOO^-$, and peroxynitrous acid, HOONO, were studied at the B3LYP/6-311+G(d,p) level of theory. It was shown that the gas-phase reactions with $ONOO^-$ proceed via an O-atom (O^3) transfer (two-electron oxidation) mechanism and produce the corresponding oxides (DMSO and DMSeO, respectively) and NO_2^- anion. The rate-determining barrier, the O−O bond cleavage, is found to be higher by 6−7 kcal/mol for DMS than for DMSe, indicating that DMSe is more reactive toward $ONOO^-$ than DMS. The inclusion of solvent effects decreases the rate-determining barrier and makes it <13.5 kcal/mol in aqueous solution for the DMS reaction. These data indicate that neither DMS nor DMSe catalyze the direct peroxynitrite → nitrate isomerization. It was shown that the reaction of DMS with *cis*-HOONO might proceed via two distinct pathways, stepwise and concerted, and is much faster than that with $ONOO^-$. The stepwise pathway starts with homolysis of the HO−ONO bond to discrete $HO^•$ and $ONO^•$ radicals, which then coordinate to DMS and produce the **$(CH_3)_2S(OH)(NO_2)$** intermediate product. This product undergoes further transformations via two different pathways: (a) a barrierless and endothermic pathway leading to the **$(CH_3)_2S(OH)^•$** and **$NO_2^•$** radicals, and (b) an exothermic H-atom transfer pathway forming DMSO and HONO via a barrier at the **TS2(H-transfer)** transition state. The $\Delta H(\Delta G)$ values of the rate-determining steps of these two pathways are 24.3 (11.0) and 11.5 (13.1) kcal/mol, respectively, in the gas phase. The concerted pathway proceeds with an O−O bond cleavage barrier of 6.1 (6.3) kcal/mol and leads to DMSO and HONO. It is predicted that the reaction of DMS with HOONO in the gas phase most likely proceeds via the stepwise (one-electron oxidation) pathway only after including entropy effects. However, in the solution phase the stepwise and concerted pathways will effectively compete with each other.

I. Introduction

Peroxynitrite[51] is a powerful inorganic oxidant, which can be formed in vivo by a diffusion-controlled[1] recombination of nitric oxide (NO) and superoxide anion ($O_2^{•-}$):

$$NO + O2^{•-} \rightarrow ONOO^-$$

Peroxynitrite anion is fairly stable in alkaline solution, but quickly ($\tau_{1/2} \sim 1.2-1.3$ s) isomerizes to nitrate upon protonation ($pK_a = 6.8$).[2−4] The aspects of the mechanism of HOONO isomerization to nitrate remain uncertain. However, on its way to nitrate, HOONO produces highly reactive "radical-like" intermediates, believed to be $^•OH$ and $NO_2^•$ radicals.[2a,5] Peroxynitrite and its related radicals ($HO^•$ and $NO_2^•$) rapidly react with numerous bio-molecules, including proteins, lipids, DNA, and aromatic compounds.[6−14] Their high reactivity and ability to cross biological membranes[7,8] implicate peroxynitrite in many disease states.[15] Accumulating evidence[16] for peroxynitrite formation in vivo has led to the search for drugs that can intercept this powerful oxidizing and nitrating agent, and detoxify it.

A series of water-soluble Fe^{III}−porphyrin complexes,[17,18] heme-containing proteins,[19] selenoproteins,[20] as well as synthetic organo-selenium compounds[21] (e.g., ebselen, [2-phenyl-1,2-benzisoselenazol-3(2*H*)-one[22]], and organo-sulfur compounds (e.g., methionine, (Met))[23] were shown to intercept, and/or to catalyze the decomposition and isomerization of peroxynitrite. For example, Met reacts[23a] with peroxynitrous acid and peroxynitrite anion with bimolecular rate constants of $(1.7 \pm 0.1) \times 10^3$ and 8.6 ± 0.2 M^{-1} s^{-1}, respectively. Interestingly, one peroxynitrite is converted to nitrate for every two sulfoxides and nitrites formed over a wide range of concentrations and pH.[23a] In other words, Met seems to catalyze the isomerization of peroxynitrite to nitrate. The mechanisms of the reaction of Met with peroxynitrite are not clear. In general, reaction may occur via one- and/or two-electron oxidation pathways. The one-electron oxidation may occur via a hydroxyl radical intermediate (possibly generated from HO−ONO homolysis) or the metastable reactive intermediate, ONOOH*.[23b,24] However, recently, the participation of free hydroxyl radicals in peroxynitrite oxidation has been called into question.[2c,25−27] Alternatively, the two-electron oxidation pathway involves O-atom transfer from peroxynitrite to sulfide to form the corresponding sulfoxide. Thus, peroxynitrite reactions with thioethers are certainly more complex than simple "oxygen atom" transfer, and the

* Corresponding author. E-mail: dmusaev@emory.edu.

10.1021/jp035144p CCC: $25.00
Published on Web 07/03/2003

elucidation of their mechanisms requires more comprehensive (both experimental and theoretical) studies.

In this paper we use density functional theory to rationalize the reactions of peroxynitrite with thioethers. Dimethylsulfide (DMS) is a simplest thioether and is the most attractive for computational studies. Therefore, in this paper we study the mechanisms of the reactions of DMS with both peroxynitrite forms, $ONOO^-$ and HOONO. Its Se analogue, dimethylselenide (DMSe), is also studied for comparison:

$$(CH_3)_2X + ONOO^- \quad (1)$$

$$(CH_3)_2X + HOONO \quad (2)$$

where X = S and Se.

A majority of the reactions of peroxynitrite with thioethers take place in hydrophobic environments or in aqueous solution with a high content of organic material, at lipid/water or on gas/liquid interfaces, and, in general, are solvent dependent. It has been shown that the decay rate of organic peroxynitrites, ROONO, in alcoholic solution is roughly 200 times greater than that in water.[1c] Also, it has been pointed out that peroxynitrite-dependent nitration of tyrosine in the aqueous phase is different from that in the membrane.[28] Therefore, elucidation of the role of solvent effects on the mechanism of the reaction of DMS with peroxynitrite is very important. In the present paper we include the solvent effects in the calculations in two different ways: using the single-point Polarizable Continuum Model[29] approach, and explicitly including several water molecules into the calculations.

Previously, several theoretical studies on the reaction of the peroxynitrite with numerous organic and inorganic molecules have been reported. Houk and co-workers[30] have investigated the reactions of peroxynitrite with amines, sulfides, alkenes, and ketones. Their B3LYP/6-31G* calculations have demonstrated[30a] that the reaction of HOONO with SH_2 has a 17.8 kcal/mol barrier for the two-electron oxidation transition state. Further, they have shown[47,30s] the existence of the hydrogen-bonded $[HO^{\bullet}\cdots NO_2^{\bullet}]$ radical pair, which is predicted to be involved in the peroxynitrite-to-nitrate isomerization and one-electron oxidation processes. However, the recent studies of Musaev and Hirao[31] using higher level methods (such as MP2 and CCSD(T)), and including entropy and explicit solvent effects in the calculations did not support the existence of this radical pair. Bach and co-workers[32] have studied the reaction of HOONO with alkenes (ethylene and propene), dimethylsulfide, trimethylamine, and trimethylphosphine at the various levels of the theory. The oxidation barriers of dimethylsulfide, trimethylamine, and trimethylphosphine by HOONO were reported to be 8.3, 4.6, and 0.5 kcal/mol at the QCISD(T)/6-31G*//B3LYP/6-311G** level of the theory.[32] Recently, Shustov and co-workers[33] applied computational methods to study the mechanism of aliphatic C−H bond oxidation in methane, propane, isobutane, propene, and 1,4-pentadiene with peroxynitrous acid and peroxynitrite anion. They have analyzed three different mechanisms, namely, (a) direct oxygen insertion into the C−H bond (two-electron oxidation), (b) H-atom abstraction (one-electron oxidation), and (c) HO−ONO bond homolysis to form hydroxyl radical. Their data include entropy effects and support mechanism (c), an involvement of discrete hydroxyl radicals in lipid peroxidation by O_2 initiated in the presence of peroxynitrite. The direct (two-electron) hydroxylation of allylic C−H bonds and C=C bond epoxidation are predicted to have higher activation energies in comparison with the energy of homolysis. Musaev and co-workers[31,34] arrived at similar conclusions on the mechanisms of the reaction of ebselen (and its derivatives) with peroxynitrite using the B3LYP/6-311+G(d,p) approach. These calculations have demonstrated that, at the enthalpy level, the two-electron oxidation of ebselen (and its derivatives) is energetically the most favorable pathway both in the gas phase and in solution. However, the inclusion of entropy corrections makes the one-electron oxidation pathway the most favorable in the gas phase.

II. Calculation Procedure

All calculations were performed using the quantum chemical package GAUSSIAN-98.[35] The geometries, vibrational frequencies, and energetics of all the reactants, intermediates, transition states, and products were calculated using hybrid density functional theory employing the B3LYP method.[36] In these calculations, we used the 6-311+G(d,p) basis set. Previous studies[30−34,37,38] have demonstrated that the B3LYP/6-311+G(d,p) approach provides excellent geometries compared with the more sophisticated approaches, such as CCSD(T), G2 and CBS-Q using the 6-311+G(d,p) basis sets. Furthermore, we[31,34] and others[32,39] have demonstrated that the B3LYP/6-311+G(d,p) approach underestimates the calculated energetic barriers by a few kcal/mol relative to the CCSD(T) and QCISD(T) methods. Since our major task in this paper is to compare the reactivity of the compounds $(CH_3)_2X$ (where X = S and Se) with HOONO and $ONOO^-$ calculated at the same (B3LYP/6-311+G(d,p)) level of theory, we believe that the underestimation of the O−O bond cleavage barriers by the B3LYP method will not affect our major conclusions. Nevertheless, for some selective structures (see below) we performed the CCSD(T), MP4(SDQ), MP3, and MP2 calculations using 6-311+G(d,p) basis sets and the B3LYP/6-311+G(d,p) optimized geometries.

The solvent effect on the mechanism of reaction 1 was examined in two different ways. First, we performed single-point Polarizable Continuum Model[29] calculations using the 6-311+G(d,p) basis set and the B3LYP/6-311+G(d,p) optimized geometries, referred to below as PCM-B3LYP/6-311+G(d,p). In these calculations we used water, dichloromethane, benzene, and cyclohexane as the solvents. Their default dielectric constants were taken from the Gaussian-98 program.[35] Second, we explicitly included several water molecules into the calculations and re-optimized geometries of the important intermediates and transition states of reaction 1 for X = S.

Note that the thermodynamic analyses were carried out at 278.15 K of temperature and 1 atm of pressure, using the principal isotope for each element type and un-scaled vibrational frequencies (all these conditions are default in the Gaussian_98 quantum chemical package,[35] that was used in these calculations).

This paper is organized as follows. Section III addresses the mechanism of reaction 1 for X = S and Se. Section IV presents studies of the mechanism of reaction between $(CH_3)_2S$ and HOONO, and Section V gives a few conclusions and predictions from these studies.

III. Reactions of $(CH_3)_2X$ (where X = S and Se) with $ONOO^-$

III.1. Gas-Phase Studies. The lowest energy structures of the reactants, $(CH_3)_2S$, $(CH_3)_2Se$ and $ONOO^-$ (PN), of reaction 1 are given in Figure 1.

PN has been the subject of many previous theoretical studies.[30−33,40] In general, we and others have identified two different isomers, cis and trans. *cis*-$ONOO^-$ is found to be 2−4 kcal/mol more stable than *trans*-$ONOO^-$ and separated from it

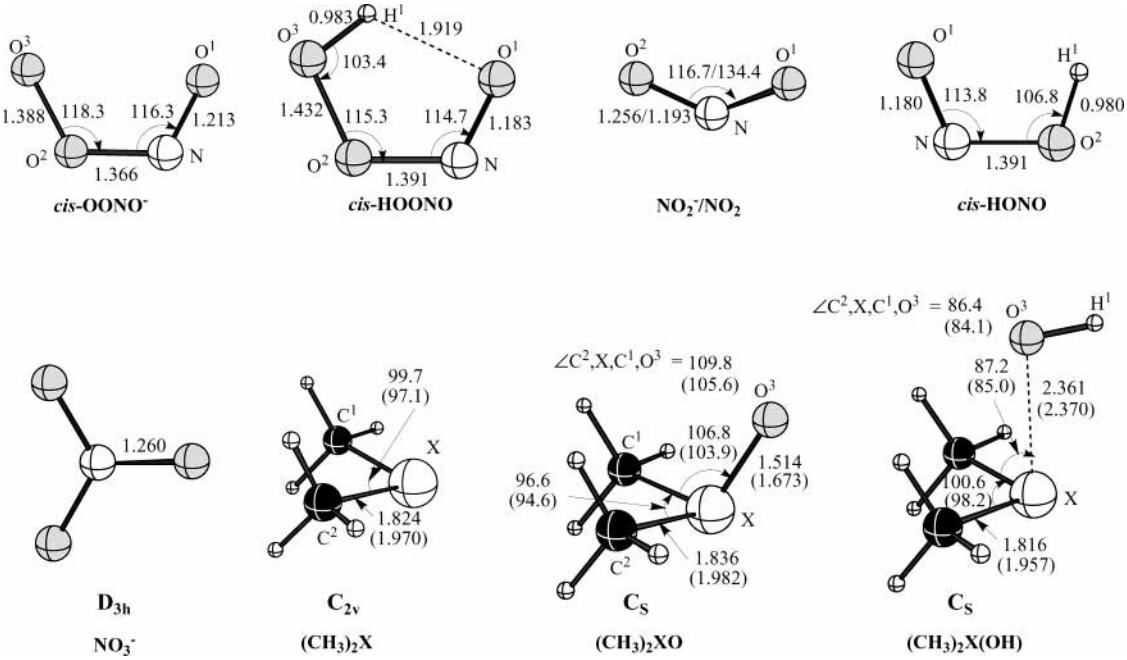

Figure 1. The B3LYP/6-311+G(d,p) calculated important geometrical parameters of the reactants and possible products of the reaction of $(CH_3)_2X$ with *cis*-$ONOO^-$ and *cis*-HOONO, where X = S and Se (in parentheses). All distances are in Å, but angles are in degrees.

by energy barrier of about 21−27 kcal/mol. In Figure 1 the structure of only *cis*-$ONOO^-$ is given, and in this paper, the reactivity of the energetically most favorable cis isomer with $(CH_3)_2S$ and $(CH_3)_2Se$ is studied. The Mulliken charges calculated at the B3LYP/6-311+G(d,p) level show the large negative charges, −0.524e and −0.366e, on the terminal oxygen atoms, O^3 and O^1, respectively (see Supporting Information, Table S3).

The structures of DMS and DMSe have also been discussed in the literature.[41,42] Our findings (Figure 1) are consistent with the previous data, and they show that these compounds have C_{2v} symmetry with the X−C bond distances of 1.824 and 1.970 Å for X = S and Se, respectively.

As expected from the charge distributions, the first step of reaction 1 is coordination of the negatively charged O^3-end of PN to the X center to form **$(CH_3)_2X$(*cis*-$ONOO^-$)** (see Figure 2).

As seen in Figure 2, where we present only the most important geometrical parameters (the Cartesian coordinates of all of the calculated structures are given in Table S1 of the Supporting Information), the coordination of *cis*-$ONOO^-$ to $(CH_3)_2X$ does not significantly change the geometries of both reactants relative to their un-complexed forms. This indicates a weak interaction between the *cis*-$ONOO^-$ and $(CH_3)_2X$.

As seen in Table 1, where we give the energies (relative to the reactants) of all the calculated intermediates, transition states, and products of reaction 1, the first step of the reaction, which is the formation of the ion−molecular complex **$(CH_3)_2X$(*cis*-$ONOO^-$)**, is exothermic by 6.4 and 6.8 kcal/mol for X = S and Se, respectively, at the ΔH level. However, the inclusion of the entropy corrections make it endothermic by (1.2) and (0.8) kcal/mol for X = S and Se, respectively. (Here and below, all numbers presented without parentheses are ΔH values, while those given in parentheses are ΔG values).

In the next step, the O^3-O^2 bond cleavage takes place at the transition state **TS1(O−O activ.)** (Figure 2), which is positively characterized by normal-mode analysis: it has only one imaginary frequency (469.1*i* cm^{-1} and 409.6*i* cm^{-1} for X = S and Se, respectively) corresponding to the O^3-O^2 bond cleavage. Intrinsic reaction coordinate[43] (IRC) calculations show that this transition state connects the pre-reaction complex **$(CH_3)_2X$-(*cis*-$ONOO^-$)** to the **$(CH_3)_2XO(NO_2^-)$** product. In this transition state, the broken O^3-O^2 bond is significantly (0.408 and 0.394 Å) elongated, while the forming $X-O^3$ bond distance is shortened by 1.672 and 2.100 Å, for X = S and Se, respectively, relative to the corresponding pre-reaction complex (see Figure 2). Furthermore, the O^1-H bond formed (from the C^1H_3 group) is also shortened by 0.749 and 1.167 Å for the X = S and Se, respectively. All these geometrical changes are consistent with the nature of this transition state, where the O^3-O^2 bond is cleaved, but the $M-O^3$ and $N^1=O^2$ double bonds are formed.

The O^3-O^2 bond cleavage barrier is 21.7 and 15.7 kcal/mol at the ΔH level for the X = S and Se, respectively, calculated from the corresponding pre-reaction complex **$(CH_3)_2X$(*cis*-$ONOO^-$)**. At the ΔG level the pre-reaction complex lies higher than reactants. Therefore, at the ΔG level the O^3-O^2 bond cleavage barrier is calculated from the reactants, and found to be (26.2) and (19.9) kcal/mol for the X = S and Se, respectively.

Overcoming the barriers at the transition state **TS1(O−O activ.)** leads to the product **$(CH_3)_2XO(NO_2^-)$**, where the product $X=O^3$ bond distance is 1.533 and 1.692 Å for X = S and Se, respectively. The NO_2 unit is bound to the **$(CH_3)_2XO$** fragment via two H-atoms of the methyl groups.

The comparison of the geometrical parameters of NO_2 unit in the product complex with those for the NO_2 and NO_2^- molecules (see Figure 1) show that bound NO_2 in **$(CH_3)_2XO(NO_2^-)$** is the nitrite anion. Thus, the product of the O^3-O^2 bond cleavage, **$(CH_3)_2XO(NO_2^-)$**, is the complex of NO_2^- with DMSO or DMSeO, respectively. This is also consistent with the Mulliken charge (see Table S3 of Supporting Information) analysis indicating an overall 0.92−0.93e negative charge on the NO_2 unit. In addition, the X-center is oxidized: the positive charge on X is 0.49 and 0.52e for X = S and Se, respectively.

The intermediate **$(CH_3)_2XO(NO_2^-)$** is lower in energy than the reactants by 51.5 (42.3) and 46.3 (38.0) kcal/mol for X = S and Se, respectively. The reaction of PN with DMS is 4.3 kcal/mol more exothermic than the corresponding reaction with DMSe, in agreement with a difference in the

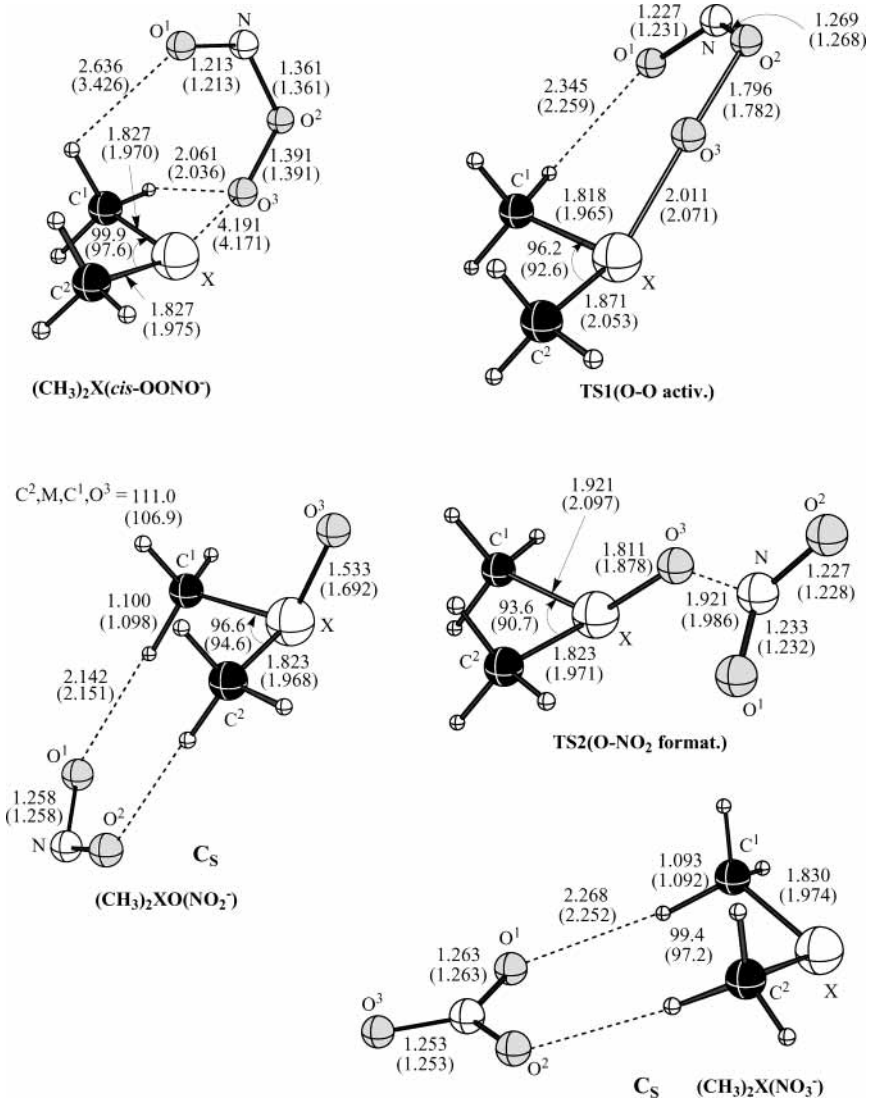

Figure 2. The B3LYP/6-311+G(d,p) calculated important geometrical parameters of all possible intermediates and transition states of the reaction of $(CH_3)_2X$ with *cis*-$ONOO^-$, where X = S and Se (in parentheses). All distances are in Å, and angles are in degrees.

TABLE 1: The Energies of the Intermediates, Transition States, and Products of the Reaction $(CH_3)_2X$ + *cis*-$ONOO^-$, Calculated at the B3LYP/6-311+G(d,p) Level of Theory[a]

structures	ΔE	ΔE + ZPC	ΔH	ΔG
		X = S		
$(CH_3)_2S$ + *cis*-$ONOO^-$	−758.437964	−758.351524	−758.341053	−758.404427
TS1 (O−O activ.)	15.4	15.3	15.3	26.2
$(CH_3)_2SO(NO_2^-)$	−52.9	−51.8	−51.5	−42.3
TS2 (O−NO_2 format.)	5.6	5.4	5.5	15.8
$(CH_3)_2S(NO_3^-)$	−62.3	−59.9	−59.5	−51.3
$(CH_3)_2SO + NO_2^-$	−34.4	−34.2	−34.2	−33.7
$(CH_3)_2S + NO_3^-$	−54.2	−52.4	−52.7	−52.2
		X = Se		
$(CH_3)_2Se$ + *cis*-$ONOO^-$	−2761.771815	−2761.686696	−2761.675896	−2761.741166
TS1 (O−O activ.)	9.3	8.8	8.9	19.9
$(CH_3)_2SeO(NO_2^-)$	−47.3	−46.7	−46.3	−38.0
TS2 (O−NO_2 format.)	−0.6	−1.2	−0.9	9.3
$(CH_3)_2Se(NO_3^-)$	−62.4	−59.9	−59.6	−51.3
$(CH_3)_2SeO + NO_2$	−28.4	−28.9	−28.7	−28.5
$(CH_3)_2Se + NO_3^-$	−54.2	−52.4	−52.7	−52.2

[a] Relative energies are in kcal/mol, but total energies of the reference structures are in hartree.

strengths of the S═O and Se═O bonds formed, which are 124.7 ± 1.0 and (111.1 ± 5.1 kcal/mol), respectively.[44]

From the resulting **$(CH_3)_2XO(NO_2^-)$** product, the reaction may split into two distinct channels: (a) dissociation into NO_2^- and $(CH_3)_2XO$ (pathway **I**), and (b) nitrate (NO_3^-) formation with recovery of starting $(CH_3)_2X$ complex (catalytic peroxynitrite → nitrate isomerization, pathway **II**).

Our calculations show that a pathway **I** is a barrierless and an endothermic process: 17.3 (8.6) and 17.6 (9.5) kcal/mol for X = S and Se, respectively. The final products ($(CH_3)_2XO$ +

TABLE 2: The Energy (in kcal/mol) of Hydration of the *cis*-$ONOO^-$, as Well as the O−O Bond Activation Barrier of the Reaction $(CH_3)_2S$ + *cis*-$ONOO^-$ Calculated at the Different Level of Theory[a]

Structures	B3LYP	CCSD(T)	MP4(SDQ)	MP3	MP2
H_2O + *cis*-$ONOO^-$	0.0	0.0	0.0	0.0	0.0
$H_2O(ONOO^-)$	−17.6	−17.7	−15.7	−19.2	−18.3
$(CH_3)_2S$ + *cis*-$ONOO^-$	0.0	0.0	0.0	0.0	0.0
$(CH_3)_2S$(*cis*-$ONOO^-$)	−6.4	−8.3	−8.1	−8.6	−8.4
TS1 (O−O activ.)	15.8	17.9	23.3	26.7	24.9

[a] In these calculations we have used B3LYP optimized geometries.

NO_2^-) lie 34.2 (33.7) and 28.7 (28.5) kcal/mol lower than reactants, for X = S and Se, respectively.

A pathway **II** starting from the same **$(CH_3)_2XO(NO_2^-)$** complex includes the transition state **TS2 (O−NO_2 format.)**. The normal-mode analysis shows that this is a real transition state with one imaginary frequency (531*i* cm^{-1} and 377*i* cm^{-1} for X = S and Se, respectively) corresponding to formation of the $N-O^3$ bond. The nascent $N-O^3$ bond distance in **TS2 (O−NO_2 format.)** is 1.921 and 1.986 Å for X = S and Se, respectively. In addition, the broken $X-O^3$ bond distance is elongated by 0.278 and 0.186 Å compared to that in the pre-reaction complex **$(CH_3)_2XO(NO_2^-)$**, for X = S and Se, respectively. IRC calculations show that the **TS2(O−NO_2 format.)** connects the complex **$(CH_3)_2XO(NO_2^-)$** with the product **$(CH_3)_2X(NO_3^-)$** (Figure 2).

The energy of the transition state **TS2(O−NO_2 format.)** is much above the corresponding pre-reaction complex **$(CH_3)_2XO(NO_2^-)$**: 57.0 (58.1) and 45.4 (47.3) kcal/mol, for X = S and Se, respectively. This makes the peroxynitrite → nitrate isomerization pathway highly unfavorable compared to an oxygen atom transfer. The resulting complex **$(CH_3)_2X(NO_3^-)$**, where the NO_3^- ligand is already formed lies 8.0 (9.0) and 13.3 (13.3) kcal/mol lower than pre-reaction complex **$(CH_3)_2XO(NO_2^-)$**, while the entire process, **$(CH_3)_2X$ + *cis*-$ONOO^-$ → $(CH_3)_2X$ + NO_3^-** is exothermic by 52.7 (52.2) kcal/mol for the both X = S and Se. The calculated $ONOO^-$ isomerization energy, 52.7 (52.2) kcal/mol in the gas phase, is close to $\Delta G° = (40.5-43.1)$ kcal/mol[45] that was experimentally estimated in water.

Summarizing this part of the paper one can conclude that, in the gas phase, reaction 1 is a two-electron oxidation process and proceeds via an O-atom transfer pathway and leads directly to the final products, $(CH_3)_2XO$ and NO_2^-. The entire reaction is exothermic by 34.2 (33.7) and 28.7 (28.5) kcal/mol for X = S and Se, respectively. The rate-determining barrier, the O−O bond cleavage, is 21.7 (26.2) and 15.7 (19.9) kcal/mol for X = S and Se, respectively. *Thus, (a) DMSe reacts faster with peroxynitrite anion than DMS, and (b) peroxynitrite → nitrate isomerization process catalyzed by DMS and DMSe is very unfavorable relative to the oxygen atom transfer process.*

III.2. Validation of the B3LYP Results. To validate our B3LYP data presented above we performed the single-point energy calculations of the reactants, pre-reaction complex **$(CH_3)_2S$(*cis*-$ONOO^-$**, and **TS1 (O−O activ.)** of reaction 1 for X = S at the more sophisticated levels of theory, CCSD(T), MP4(SDQ), MP3, and MP2 (see Table 2).

As seen in Table 2, the B3LYP method provides results close to the CCSD(T), while it underestimates the calculated O−O bond cleavage barrier by 5 kcal/mol. However, we believe that this underestimation will not affect our final conclusions (see the Computational Procedure).

III.3. The Solvent Effects. At first, let us discuss the PCM results. In Table 3 we present the ΔG(solution) values for reaction 1 calculated at the PCM level which can be compared to the corresponding ΔE values in the gas phase. This comparison shows that including bulk solvent effects into the calculations results in more stabilization of the reactants and products of reaction 1 than the intermediates and transition states. As a result, the pre-reaction complex **$(CH_3)_2X$(*cis*-$ONOO^-$)** becomes unstable relative to the reactants, and the rate-determining O−O bond cleavage barrier increases slightly. Furthermore, dissociation of the **$O(CH_3)_2X(NO_2^-)$** complex to $(CH_3)_2XO$ and NO_2^- becomes more favorable than its transformation to nitrate and $(CH_3)_2X$. These changes are more profound in polar solvents (such as water). The overall exothermicity of reaction 1 changes only slightly.

At the next stage, we explicitly included several water molecules into calculations in order to elucidate whether water (solvent) molecules are directly involved in the reaction. Our calculations (not presented here) show that the water molecules coordinate to the peroxynitrite anion stronger than to DMS or DMSe because of the large negative charge of the former.

As seen in the Figure 4, where we present the calculated structures of the **$(H_2O)_n$(*cis*-$ONOO^-$)** complexes for $n = 1-4$, the water molecules preferably coordinate to the most negatively charged O^3 atom of the OONO-unit. For $n = 1$, the H^2-O^3 distance (where H^2 is a coordinated hydrogen atom of the first water molecule) is 1.670Å. In the case of $n = 2$, where both water molecules are simultaneously coordinated to the O^3-atom, the H^2-O^3 distance is elongated to 1.893 Å because of the formation of H^4-O^3 (where H^4 is a coordinated hydrogen atom of the second water molecule) and H^3-O (of the second H_2O molecule) forms hydrogen-bonds with lengths of 1.764 and 2.237 Å, respectively. In this case there also exists a weak H^5-O^1 interaction with bond distance of 2.609 Å.

For the complexes **$(H_2O)_n$(*cis*-$ONOO^-$)** with $n = 3$ and 4 we have located two isomers. In isomer_1, all water molecules are clustered in the vicinity of the O^3-atom; in isomer_2, one of the water molecules coordinates to the $N-O^1$ bond. Isomer_2 is about 5−6 kcal/mol higher in energy than isomer_1, and, therefore, will not be discussed below.

In Table 4 we present the calculated sequential hydration energies of the *cis*-$ONOO^-$, (e.g., energy of the reaction **$(H_2O)_n$-**

TABLE 3: The ΔG(solution) Energies (relative energies are in kcal/mol, but total energies of the reference structures are in hartree) of the Reactants, Intermediates, Transition States and Products of the Reaction $(CH_3)_2X$ + *cis*-$ONOO^-$, Calculated at the PCM-B3LYP/6-311+G(d,p)//B3LYP/6-311+G(d,p) Level

	X = S				X = Se			
structures	C_6H_{12}	C_6H_6	CH_2Cl_2	H_2O	C_6H_{12}	C_6H_6	CH_2Cl_2	H_2O
$(CH_3)_2X$ + *cis*-$ONOO^-$	−758.48811	−758.48935	−758.52709	−758.54565	−2761.81596	−2761.81739	−2761.85459	−2761.871842
$(CH_3)_2X$(*cis*-$ONOO^-$)	0.2	0.4	3.2	10.1	−0.1	0.1	3.2	6.9
TS1 (O−O activ.)	23.8	23.6	26.6	30.4	15.5	15.5	18.4	18.2
$(CH_3)_2XO(NO_2^-)$	−42.3	−42.2	−37.1	−30.5	−40.2	−40.1	−36.5	−36.1
TS (O−NO_2 format.)	16.2	16.1	20.5	−26.4	5.8	5.8	7.9	7.3
$(CH_3)_2X(NO_3^-)$	−54.2	−54.0	−49.8	−44.5	−55.1	−55.0	−51.4	−49.1
$(CH_3)_2XO$ + NO_2^-	−33.9	−34.5	−35.6	−34.5	−31.1	−31.4	−33.8	−34.8
$(CH_3)_2X$ + NO_3^-	−53.9	−53.9	−53.3	−51.5	−53.9	−53.9	−53.3	−51.5

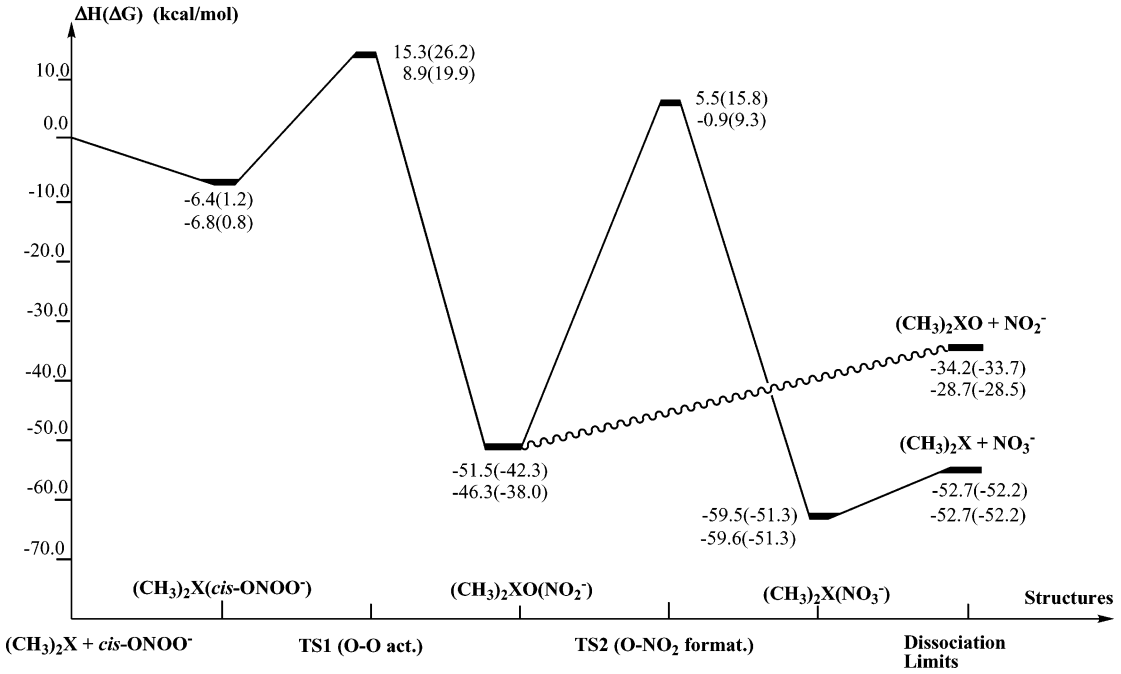

Figure 3. Schematic presentation of potential energy surface (PES) of the reaction $(CH_3)_2X$ + *cis*-$ONOO^-$ for X = S (first row) and Se (second row). Numbers given without parentheses are ΔH values, while numbers presented in parentheses correspond to ΔG values. This scheme is scaled for the ΔH values of the reaction $(CH_3)_2S$ + *cis*-$ONOO^-$.

(*cis*-$ONOO^-$) → $(H_2O)_{n-1}$(*cis*-$ONOO^-$) + H_2O), which is also presented graphically in Figure 5.

As seen from the Table 4 and Figure 5, the ΔH and ΔG values of the sequential hydration of *cis*-$ONOO^-$ decreases upon increasing *n*: ΔH values are 16.3, 14.3, 11.8, and 11.8 kcal/mol, while ΔG values are 9.0, 4.0, 3.0, and 2.6 kcal/mol, for $n = 1$, 2, 3, and 4, respectively.

In water the reaction of DMS with *cis*-$ONOO^-$ becomes the reaction of the DMS with hydrated *cis*-$ONOO^-$, **$(H_2O)_n$(*cis*-$ONOO^-$)**. Therefore, one should study reaction 3

$$(CH_3)_2X + (H_2O)_n(cis\text{-}ONOO^-) \qquad (3)$$

In this paper we study only the rate-determining O−O bond cleavage (including reactants, pre-reaction complex, and O−O bond cleavage transition state) of reaction 3 for $n = 1$ and 2, and X = S. The calculated structures and energetics of **$(CH_3)_2S(H_2O)_n$(*cis*-$ONOO^-$)** intermediates and O−O bond cleavage transition states are given in Figure 6 and Table 4, respectively.

A comparison of the important geometrical parameters of pre-reaction complexes and O−O bond cleavage transition states of reactions 1 and 3 (presented in Figures 2 and 6, respectively) shows that the explicit inclusion of water molecules in the reaction significantly affects the calculated $X-O^3$ distance in the pre-reaction complexes. At the same time, in **TS1** the important $S-O^3$ and O^3-O^2 bond distances elongate by 0.141 and 0.012 Å for $n = 1$, and 0.208 and 0.010 Å for $n = 2$, respectively.

Thus, the hydration of *cis*-$ONOO^-$ makes the **TS1** more "reactant-like", and shifts the equilibrium in favor of the reactants. Indeed, ΔH of **$(CH_3)_2S(H_2O)_n$(*cis*-$ONOO^-$)** formation becomes more positive with the increasing of *n*: −6.4, −4.6, and +0.1 kcal/mol for $n = 0$, 1, and 2, respectively. Extrapolation of these data to $n > 2$ indicates that **$(CH_3)_2S(H_2O)_n$(*cis*-$ONOO^-$)** will be unstable, and, therefore, rate-determining O−O bond cleavage barrier should be calculated relative to the reactants, rather than from the pre-reaction complex **$(CH_3)_2S(H_2O)_n$(*cis*-$ONOO^-$)**.

As seen in Tables 1 and 4, the enthalpy of O−O bond cleavage calculated from the reactants is 15.3, 14.7, and 13.5 kcal/mol for $n = 0$, 1, and 2, respectively. Extrapolation of these data to $n > 2$ indicates that at larger values of *n* the barrier for O−O bond cleavage in *cis*-$ONOO^-$ by DMS will be even smaller. In the other words, *water molecules reduce the rate-determining O−O bond cleavage barrier of reaction 3, e.g., they facilitate it. Here, we predict that the O−O bond cleavage barrier in PN by DMS will be less than 13.5 kcal/mol in water.*

We did not study the explicit solvent effect on the mechanism of reaction 1 for X = Se, but it is likely to be very similar to the case of DMS.

Thus, our explicit solvent studies show that the hydration of PN reduces the acidity of its O^3-center, resulting in the lowering of the O-atom transfer (or O−O bond cleavage) barrier. Water also destabilizes the pre-reaction complex and makes it unstable relative to the reactants. In general, similar effects should be expected from the PCM studies, which take into account the bulk solvent effects. Indeed, similar to the explicit solvent studies, the PCM significantly destabilizes the pre-reaction complex. However, contrary to the explicit solvent studies, PCM calculations predict an increase in the O−O bond cleavage barrier. This discrepancy between the PCM and explicit solvent studies is likely due to the use of the B3LYP/6-311+G(d,p) gas-phase geometries in PCM calculations.

IV. Reaction of DMS with HOONO

Theoreticians have already extensively studied the peroxynitrous acid, HOONO.[26,32,46] It was shown that the cis-perp and cis-cis isomers of this molecule, which differ from each other by rotation (about 90−100 deg.) around the O−H bond, are energetically the lowest ones. The cis-cis isomer is predicted to be 0.5−1.5 kcal/mol lower in energy (ΔE values) than the cis-perp isomer at different levels of the theory (MP2, QCISD(T), CCSD(T), G2, and CBS-APNO). Our B3LYP/6-311+G-

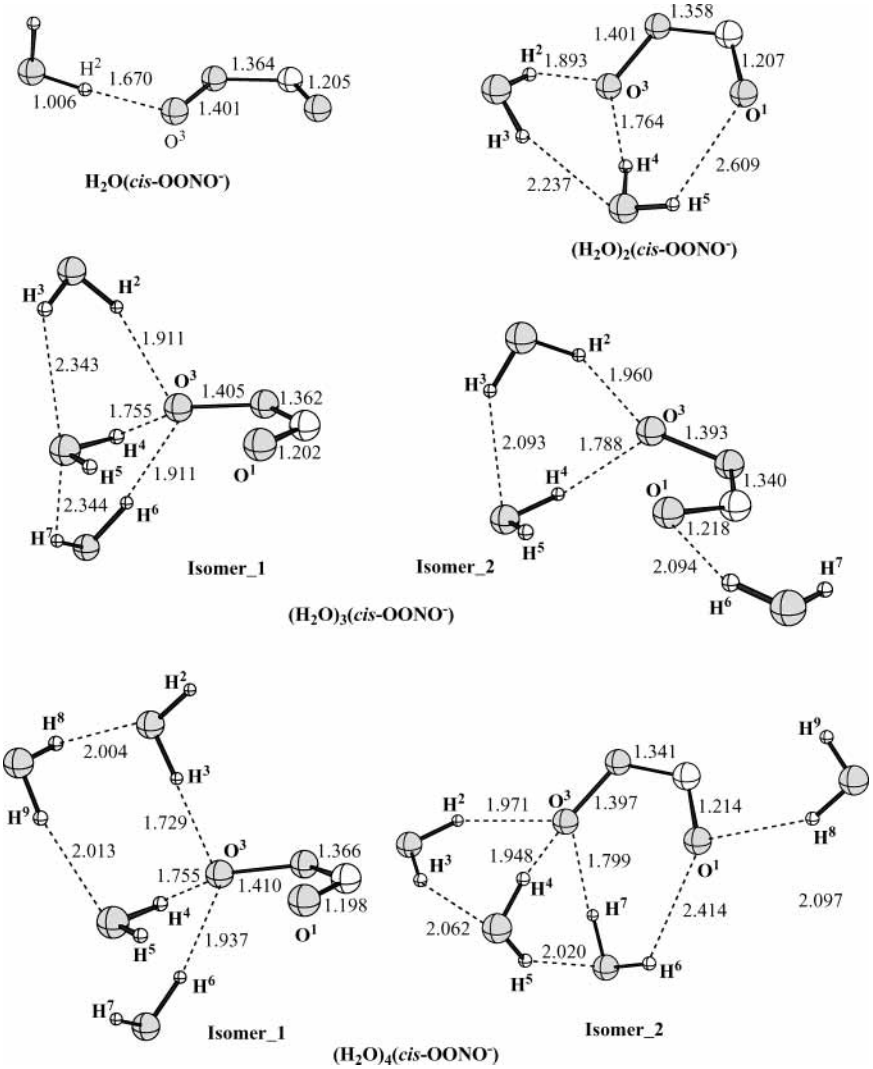

Figure 4. The B3LYP/6-311+G(d,p) optimized structures of the $(H_2O)_n$(*cis*-$ONOO^-$) (where $n = 1$, 2, 3, and 4) and their important geometrical parameters. All distances are in Å.

TABLE 4: The Sequential Hydration Energy of the *cis*-$ONOO^-$ Anion [$(H_2O)_n$(*cis*-$ONOO^-$) → $(H_2O)_{n-1}$(*cis*-$ONOO^-$) + H_2O], as Well as the Relative Energies of the Intermediates, Transition States, and Products of the Reaction $(CH_3)_2S$ + $(H_2O)_n$(*cis*-$OONO^-$) Calculated at the B3LYP/6-311+G(d,p) Level of Theory[a]

structures	ΔE	ΔE + ZPC	ΔH	ΔG
H_2O + *cis*-$ONOO^-$	−356.829734	−356.797346	−356.788967	−356.840790
(H_2O)(*cis*-$ONOO^-$)	−17.6	−15.9	−16.3	−9.0
H_2O + (H_2O)(*cis*-$ONOO^-$)	−433.316285	−433.259869	−433.248253	−433.310001
$(H_2O)_2$(*cis*-$ONOO^-$)	−16.3	−13.4	−14.3	−4.0
H_2O + $(H_2O)_2$(*cis*-$ONOO^-$)	−509.800756	−509.718336	−509.704350	−509.771125
$(H_2O)_3$(*cis*-$ONOO^-$)	−13.6	−11.3	−11.8	−3.0
H_2O + $(H_2O)_3$(*cis*-$ONOO^-$)	−586.280818	−586.173544	−586.156573	−586.230750
$(H_2O)_4$(*cis*-$ONOO^-$)	−13.7	−11.1	−11.8	−2.6
$(CH_3)_2S$ + (H_2O)(*cis*-$ONOO^-$)	−834.924515	−834.814047	−834.800339	−834.873638
$(CH_3)_2S(H_2O)$(*cis*-$ONOO^-$)	−5.8	−5.3	−4.6	3.0
TS1_H_2O (O−O activ.)	14.2	15.0	14.7	27.6
$(CH_3)_2S$ + $(H_2O)_2$(*cis*-$ONOO^-$)	−911.408986	−911.275140	−911.256436	−911.334762
$(CH_3)_2S(H_2O)_2$(*cis*-$ONOO^-$)	−1.3	−0.2	0.1	6.2
TS1_$(H_2O)_2$ (O−O activ.)	13.2	13.8	13.5	25.5

[a] All relative energies are in kcal/mol and relative to the reactants the given total electronic and Gibbs free energies of the reactants are in hartree.

(d,p) calculations show that the cis-cis isomer is lower by 0.5 kcal/mol than the cis-perp isomer at the ΔH level. However, the inclusion of entropy effects makes the cis-perp isomer lower by only 0.1 kcal/mol than the cis-cis isomer. Since these two isomers are practically degenerate in energy and can easily rearrange to each other,[46] we study reaction 2 (discussed below) for the cis-cis isomer of HOONO. Subsequently, for simplicity, we refer to *cis*-*cis*-HOONO as "*cis*-HOONO" (see also Figure 1).

In general, the reaction of DMS with HOONO (eq 2) may proceed via two pathways: stepwise and concerted. First, we address the concerted pathway. The calculated important geo-

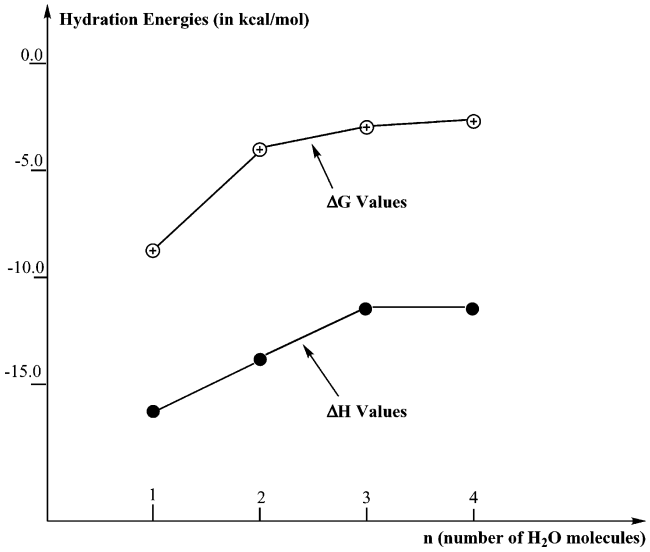

Figure 5. Graphical representation of the calculated sequential hydration energies of the peroxynitrite anion, i.e. reaction *cis*-$ONOO^-$ + $n(H_2O)$ → $(H_2O)_n$(*cis*-$ONOO^-$).

metrical parameters of the intermediates, transition states, and products of reaction 2 for X = S are shown in Figure 7. Their relative energies are presented in Table 5.

As seen in Figure 7, in the pre-reaction **$(CH_3)_2S$(*cis*-HOONO)** complex the *cis*-HOONO molecule coordinates to the S-center via its H-atom: the $S-H^1$ distance is 2.243 Å. Such an interaction results in significant changes of the geometries of the *cis*-HOONO molecule. At first, the intramolecular H^1-O^1 interaction in free *cis*-HOONO is completely destroyed and the OH-group is rotated, becoming almost perpendicular to the $O^3O^2NO^1$-plane. Second, the $N-O^2$ bond is elongated by 0.072Å compared to that of the free *cis*-HOONO molecule. The geometry of the $(CH_3)_2S$ fragment in the complex with *cis*-HOONO is almost the same as that of free DMS, and, therefore, will not be discussed.

The calculated **$(CH_3)_2S$ + *cis*-HOONO → $(CH_3)_2S$(*cis*-HOONO)** complexation energy is 10.2(1.0) kcal/mol (Table 5).

The next step of the reaction is HO^3-O^2 bond cleavage at the **TS1(O−O activ.)** transition state, which is confirmed to be a real transition state with one imaginary frequency of 411.2*i* cm^{-1}. Normal-mode analyses shows that this imaginary frequency corresponds to the HO^3-O^2 bond cleavage. In **TS1** the broken HO^3-O^2 bond is elongated by 0.333 Å, and the $N-O^2$ bond (π-bond) that is formed is shortened by 0.192 Å relative to their values in the pre-reaction **$(CH_3)_2S$(*cis*-HOONO)** complex. The nascent $S-O^3H$ bond has a distance of 2.395 Å. The HO^3-O^2 bond cleavage barrier is 6.1 (7.3) kcal/mol relative to the pre-reaction complex **$(CH_3)_2S$(*cis*-HOONO)**.

Intrinsic reaction coordinate (IRC) calculations show that the product of the HO^3-O^2 bond cleavage is the complex **$(CH_3)_2S$(O)(*cis*-HONO)**, where *cis*-HONO fragment is H-bound to the O^3-atom of the $(CH_3)_2SO$ fragment. The calculated O^3-H^1 and O^1-H^1 distances are 1.648 and 1.013 Å, respectively. As seen in Table 5, the complex **$(CH_3)_2S$(O)(*cis*-HONO)** is stable by 10.9 (1.5) kcal/mol relative to the dissociation limit of $(CH_3)_2SO$ + *cis*-HONO. The entire reaction $(CH_3)_2S$ + *cis*-HOONO → $(CH_3)_2SO$ + *cis*-HONO is exothermic by 32.4 (31.6) kcal/mol.

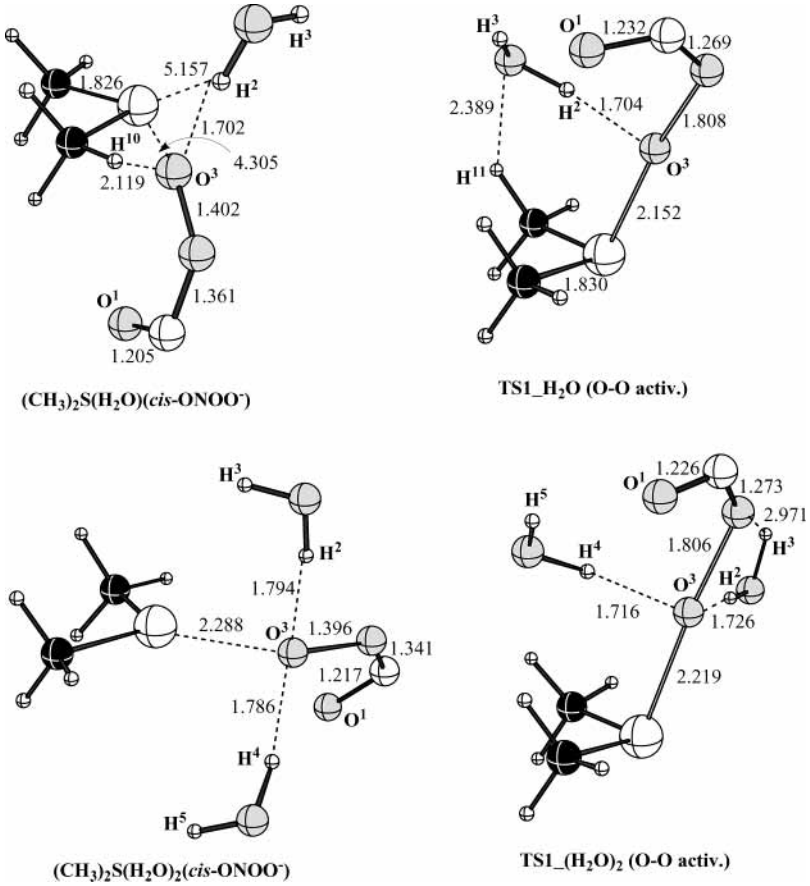

Figure 6. The B3LYP/6-311+G(d,p) calculated important geometrical parameters of the pre-reaction complexes $(CH_3)_2S[(H_2O)_n$(*cis*-$ONOO^-)]$ and O−O bond activation transition states (**TS1**) for $n = 1$ and 2. All distances are in Å.

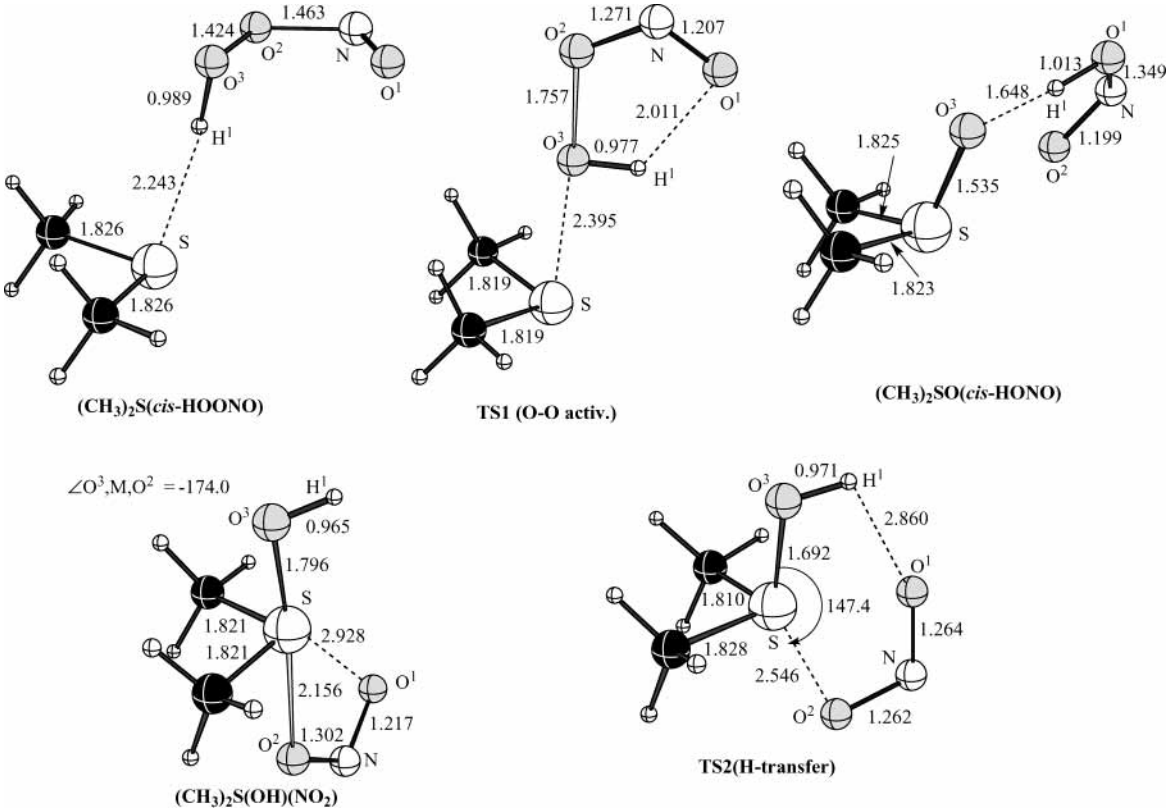

Figure 7. The B3LYP/6-311+G(d,p) calculated important geometrical parameters of the all possible intermediates and transition states of the reaction of $(CH_3)_2S$ with *cis*-HOONO. All distances are in Å.

TABLE 5: The Energies of the Intermediates, Transition States, and Products of the Reaction $(CH_3)_2S$ + *cis*-HOONO, Calculated at the B3LYP/6-311+G(d,p) Level of Theory

structures	ΔE	ΔE + ZPC	ΔH	ΔG
$(CH_3)_2S$ + *cis*-HOONO	−758.985800	−758.887380	−758.876369	−758.940726
$(CH_3)_2S$(*cis*-HOONO)	−11.0	−10.3	−10.2	−1.0
TS1 (O−O activ.)	−4.4	−4.1	−4.1	6.3
$(CH_3)_2S(OH)(NO_2)$	−30.5	−28.7	−28.7	−17.1
TS2 (H-transfer)	−18.1	−16.6	−17.2	−4.0
$(CH_3)_2SO$(*cis*-HONO)	−44.9	−43.4	−43.3	−33.1
$(CH_3)_2SO$ + *cis*-HONO	−32.6	−32.3	−32.4	−31.6
$(CH_3)_2SOH + NO_2$	−3.8	−5.2	−4.4	−6.1

[a] Relative energies are in kcal/mol, but total energies of the reference structures are in hartree.

The first step of the alternative stepwise pathway is HO−ONO homolysis to yield two radicals, $HO^\bullet$ and $NO_2^\bullet$, which proceeds with an energy of 12.3 (2.2) kcal/mol in the gas phase, as shown by the B3LYP/6-311+G(d,p) level calculations. The previous calculations at the various levels of theory predicted a homolysis HO−ONO bond enthalpy in the gas phase of 20−22 kcal/mol.[47,48] Recently, Janoschek and co-workers[49] have reported ΔH and ΔG values of 18.6 and (8.3) kcal/mol for HO−ONO homolysis in the gas phase using the more sophisticated G3MP2B3 method. The experimentally reported enthalpy and Gibbs free energy of HO−ONO homolysis are 21 ± 3 and 11 ± 3 kcal/mol, in the gas phase, and 18 ± 1 and 17 ± 1 kcal/mol in water, respectively.[27] These data clearly show that (a) the entropy effect is significantly smaller in water than in the gas phase, and (b) the B3LYP/6-311+G(d,p) approach underestimates the HO−ONO homolysis by 6−7 kcal/mol and should be used with great care.

In the next step the $HO^\bullet$ and $NO_2^\bullet$ radicals formed coordinate to DMS step-by-step and/or simultaneously to form the **$(CH_3)_2S(OH)^\bullet$**, **$(CH_3)_2S(NO_2)^\bullet$**, and **$(CH_3)_2S(OH)(NO_2)$** products, respectively. Since our calculations show that $HO^\bullet$ coordinates to DMS a few kcal/mol more strongly than $NO_2^\bullet$, below we will not discuss the structure and energetics of the less stable **$(CH_3)_2S(NO_2)$** complex. The **$(CH_3)_2S(OH)^\bullet$** complex, the structure of which is given in Figure 1, is 16.7(8.3) kcal/mol stable relative to the dissociation limit $(CH_3)_2S + HO^\bullet$. Meanwhile, the radicals $(CH_3)_2S(OH)^\bullet + NO_2^\bullet$ lie 4.4(6.1) kcal/mol lower than reactants $(CH_3)_2S$ + *cis*-HOONO, and their recombination gives the complex **$(CH_3)_2S(OH)(NO_2)$**, with the $S-O^3H$ and $S-O^2NO^1$ bonds of 1.796 and 2.156 Å, respectively. This complex lies by 28.7 (17.1) and 41.0 (19.3) kcal/mol lower than $(CH_3)_2S$ + *cis*-HOONO and $(CH_3)_2S + HO^\bullet + NO_2^\bullet$ dissociation limits, respectively. The **$(CH_3)_2S(OH)(NO_2)$** product decays via two distinct pathways. The first one, called the dissociative or "radical" pathway, is a reverse process to the $NO_2^\bullet$ coordination and leads to $NO_2^\bullet$ and $(CH_3)_2S(OH)^\bullet$ radicals. Our calculations show that this process is endothermic by 24.3 (11.0) kcal/mol. The dissociation of **$(CH_3)_2S(OH)(NO_2)$** to $HO^\bullet$ and $(CH_3)_2S(NO_2^\bullet)$ is expected to be slightly less favorable and will not be discussed.

The second process starts from the same **$(CH_3)_2S(OH)(NO_2)$** complex, the H-atom transfer pathway, proceeds via the H-atom transfer from the OH to ONO fragment, and leads to the **$(CH_3)_2S(O)$(*cis*-HONO)** complex discussed above. The reaction

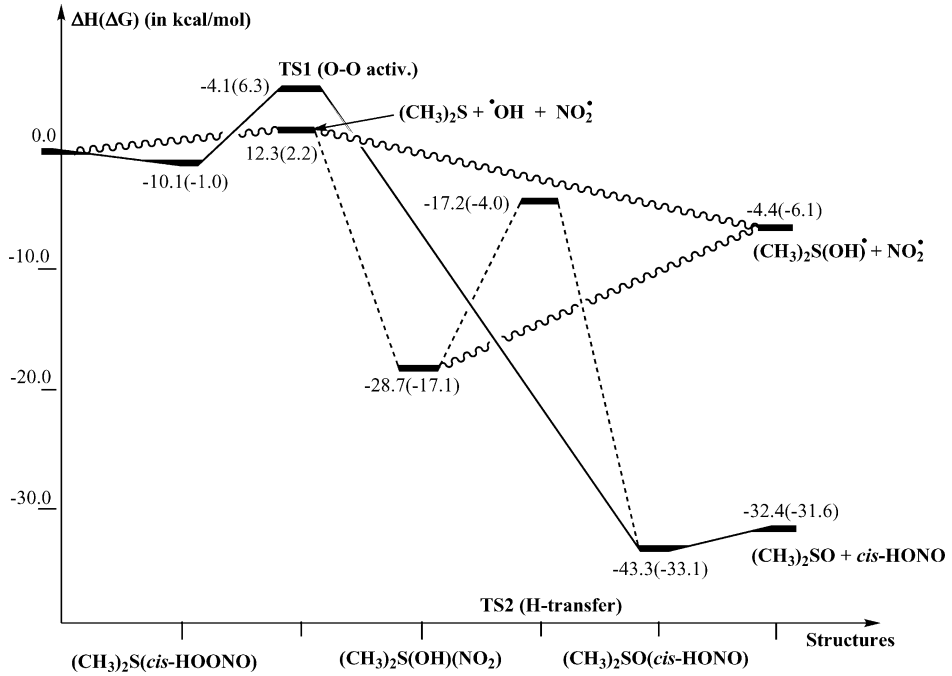

Figure 8. Schematic presentation (based on Δ*G* values) of potential energy profile of the reaction $(CH_3)_2S$ with *cis*-HOONO in the gas phase. Numbers presented here were calculated at the B3LYP/6-311+G(d,p) level. Numbers given without parentheses are Δ*H* values, while those in parentheses are Δ*G* values.

$(CH_3)_2S(OH)(NO_2)$ → $(CH_3)_2S(O)$(*cis*-HONO) is exothermic by 14.6 (16.0) kcal/mol, and proceeds with a 11.5 (13.1) kcal/mol H-atom transfer barrier at the **TS2(H-transfer)** transition state, where the O^1 atom of the O^1NO^2 fragment is coordinated to the H^1-atom of the O^3H^1-unit. In the **TS2(H-transfer)** transition state, the O^1-H^1 bond is 2.860 Å, while the broken $S-O^2$ bond is elongated by 0.39 Å compared to that in the complex **$(CH_3)_2S(OH)(NO_2)$**. These changes in $S-O^2$ and O^1-H^1 distances correlate with a decrease in the $N-O^2$ bond distance by 0.040Å, but an elongation of the $N-O^1$ bond by 0.047 Å. Normal-mode analysis shows that the **TS2(H-transfer)** is a real transition state with one ($139.1i$ cm^{-1}) imaginary frequency. Furthermore, IRC calculations confirmed that **TS2** connects **$(CH_3)_2S(OH)(NO_2)$** with the product **$(CH_3)_2S(O)$(*cis*-HONO)**.

Comparison of these two processes starting with the complex **$(CH_3)_2S(OH)(NO_2)$** shows that the dissociation of the NO_2 unit is a barrierless, but endothermic (24.3 (11.0) kcal/mol) reaction. In contrast, the H-atom transfer pathway is exothermic by 14.6 (16.0) kcal/mol, but proceeds with an activation barrier of 11.5 (13.1) kcal/mol. Thus, at the Δ*H* level, a high endothermicity of the dissociation (radical) pathway and low activation energy of H-atom transfer (sulfoxidation) makes the sulfoxidation much more likely to occur in the gas phase. However, the inclusion of the entropy corrections in the gas phase makes the NO_2 dissociation slightly (by 2.1 kcal/mol) more favorable than the unimolecular H-atom transfer process. A competition between these two pathways should be mostly determined by further reactions of the product $(CH_3)_2S(OH)^\bullet$ and $NO_2^\bullet$ radicals.

The overall potential energy surface of the reaction of DMS with ***cis*-HOONO** consists of both the concerted and stepwise pathways and is shown in Figure 8.

As seen from this Figure, the O−O bond cleavage on the concerted pathway occurs with 6.1 kcal/mol barrier, calculated from the pre-reaction complex **$(CH_3)_2S$(*cis*-HOONO)**. The inclusion of the entropy effect destabilizes the pre-reaction **$(CH_3)_2S$(*cis*-HOONO)** complex and **TS1(O−O activ.)** and shifts the **TS1(O−O activ.)** transition state by (6.3) kcal/mol higher than reactants. At the same time, the stepwise mechanism occurs with 12.3 kcal/mol enthalpy, while the inclusion of entropy reduces it to only (2.2) kcal/mol. The comparison of these data shows that, in the gas phase, reaction 2 most likely will proceed by the concerted pathway at the Δ*H* level. However, the inclusion of entropy corrections (Δ*G* values) could make the stepwise pathway favorable in the gas phase. As mentioned above, the B3LYP/6-311+G(d,p) approach used in this paper underestimates both the concerted O−O bond cleavage barrier and the HO−ONO bond homolysis. However, the value of these under-estimations are shown to be similar (5−7 kcal/mol), and therefore, unlikely to affect the conclusion above.

It is worth mentioning that the **$(CH_3)_2S(OH)^\bullet$** and $NO_2^\bullet$ radicals formed on the stepwise pathway could also be formed during the concerted pathway. The transition state (TS1′) leading to these products on the concerted pathway is expected to be energetically higher than **TS1(O−O activ.)** reported in this paper. Here, TS1′ was not located. However, in solution TS1′ could be more stabilized than **TS1(O−O activ.)**. To resolve this uncertainty, one should optimize the geometries of all the intermediates and transition states of reaction 2 in water using both the PCM and explicit water approaches. These investigations are in progress.

We also would like to mention that the stepwise mechanism is kinetically completely different from the concerted one. In the stepwise mechanism, the rate-limiting step is a unimolecular process, which is independent of DMS concentration. While, the concerted pathway should obey a first-order reaction rate law with respect to both HOONO and DMS concentrations. Therefore, a stepwise pathway could dominate at low DMS concentrations, while a concerted one could dominate at high DMS concentrations.

The single-point PCM calculations performed at the B3LYP/6-311+G(d,p) optimized geometries show that the inclusion of the solvent effects destabilizes the **$(CH_3)_2S$(*cis*-HOONO)** complex and the **TS1 (O−O activ.)** transition state relative to the reactants, and only slightly changes the O−O activation

TABLE 6: The Δ*G*(solution) Energies of the Reactants, Intermediates, Transition States, and Products of the Reaction $(CH_3)_2S$ + *cis*-HOONO, Calculated at the PCM-B3LYP/6-311+G(d,p) Level

structures	C_6H_{12}	C_6H_6	CH_2Cl_2	H_2O
$(CH_3)_2S$ + *cis*-HOONO	−758.997584	−758.994341	−759.001465	−759.003261
$(CH_3)_2S$(*cis*-HOONO)	−3.5	−3.8	−2.9	0.8
2TS1 (O−O activ.)	2.3	1.8	1.8	3.7
$(CH_3)_2S(OH)(NO_2^-)$	−26.5	−27.1	−27.7	−26.0
TS2 (H-transfer)	−12.9	−13.9	−15.1	−14.9
$(CH_3)_2SO$(*cis*-HONO)	−37.5	−38.2	−37.6	−34.0
$(CH_3)_2SO$ + *cis*-HONO	−26.7	−27.1	−28.1	−28.7
$(CH_3)_2S(OH)$ + NO_2	1.8	1.8	1.7	3.2

barrier (see Table 6). Combining this finding with the fact that in solutions the entropy contributions to the energetics of the reaction are going to be smaller than in the gas phase, one may expect that both concerted and stepwise pathways of reaction 2 are likely to be feasible.

Furthermore, the solvent effects significantly destabilize the dissociation of the **$(CH_3)_2S(OH)(NO_2)$** complex to radicals and, consequently, render the H-atom transfer (sulfoxidation) pathway even more favorable. Indeed, the barrier (Δ*E* values) of the H-atom transfer process at the transition state **TS2 (H-transfer)** is found to be 12.4, 13.6, 13.2, 12.6, and 11.1 kcal/mol in the gas phase, in cyclohexane, benzene, dichloromethane, and water, respectively, relative to the **$(CH_3)_2S(OH)(NO_2)$** complex. At the same time, NO_2 dissociation from the **$(CH_3)_2S(OH)(NO_2)$** complex is 26.7, 28.3, 28.9, 29.4, and 29.2 kcal/mol in the gas phase, in cyclohexane, benzene, dichloromethane, and water, respectively.

As mentioned above, the presented data are obtained at the PCM level using the B3LYP/6-311+G(d,p) optimized geometries, which do not take into account the geometry relaxation and entropy corrections in solution. In fact, the free energies of hydration ΔG°_{g-aq} of $(CH_3)_2S(OH)^\bullet$ and $NO_2^\bullet$ are negative, −12 ± 3)[50a] and −3 kcal/mol,[50c] respectively. Thus, the endothermicity of the dissociation pathway can be even lower in aqueous solutions, making it very competitive to sulfoxidation.

Finally, let us compare our results on the reaction DMS + HOONO with those of Bach and co-workers,[32] who have found only the concerted pathway for reaction 2 and located the corresponding transition state **TS1**. In agreement with our data they concluded that the products should be exclusively DMSO and HONO. The barrier height (Δ*E* value), 1.8 and 8.3 kcal/mol, calculated at the B3LYP/6-311G(d,p) and QCISD(T)/6-31G(d)//B3LYP/6-311G(d,p) levels, respectively, is in very good agreement with our data (Δ*E* value, 6.6 kcal/mol), obtained at the B3LYP/6-311+G(d,p) level. Furthermore, their B3LYP/6-311G(d) and MP2(full)/6-31G(d) optimized geometries of the **TS1** are also very close to our data obtained at the B3LYP/6-311+G(d,p) level.

V. Conclusions and Predictions

From the results and discussions presented above one can make the following conclusions and predictions.

(1) In the gas phase, the reaction of DMS (and DMSe) with peroxynitrite anion, $ONOO^-$, proceeds by an O-atom transfer mechanism and produces DMSO (and DMSeO) and NO_2^- anion. The O−O bond cleavage barrier at the **TS1 (O−O activ.)** transition state is 21.7 (26.2) and 15.7 (19.9) kcal/mol, while the overall exothermicity of the reaction is 34.2 (33.7) and 28.7 (28.5) kcal/mol for X ═S and Se, respectively. Thus, $ONOO^-$ should react faster with DMSe than with DMS. Both DMS and DMSe are unlikely to catalyze the isomerization of peroxynitrite to nitrate.

(2) The inclusion of solvent effects reduces the acidity of the transferred O^3 atom to the DMS and decreases the rate-determining barrier, thus, accelerating the reaction. The explicit inclusion of water molecules ($n = 1-2$) into calculations reduces the enthalpy of the O−O bond cleavage: 15.3, 14.7, and 13.5 kcal/mol (relative to the reactants) for $n = 0$, 1, and 2, respectively. In water the O−O bond cleavage barrier of the reaction of *cis*-$ONOO^-$ with DMS is likely to be smaller than 13.5 kcal/mol.

(3) Further reduction of the acidity of O^3-atom in $ONOO^-$ by its protonation (which corresponds to a decrease in pH in water), significantly reduces the O−O cleavage barrier. The reaction of DMS with *cis*-HOONO proceeds much faster than with *cis*-$ONOO^-$.

(4) The reaction DMS + *cis*-HOONO may proceed via two pathways, stepwise and concerted, both are feasible in solution.

(5) The stepwise pathway starts with HO−ONO bond homolysis to form discrete $HO^\bullet$ and $ONO^\bullet$ radicals. Both radicals coordinate to DMS and generate the intermediate **$(CH_3)_2S(OH)(NO_2)$**, which can undergo further transformation through two different pathways: dissociation to $(CH_3)_2S(OH)^\bullet$ and $NO_2^\bullet$ radicals, and H-atom transfer (sulfoxidation) to form DMSO and HONO via **TS2(H-transfer)** transition state. The first pathway is barrierless, but endothermic (24.3 (11.0) kcal/mol); the second pathway is exothermic by 14.6 (16.0) kcal/mol, but proceeds with an activation barrier of 11.5 (13.1) kcal/mol. A competition between these two pathways should be mostly determined by further reactions of the product $(CH_3)_2S(OH)^\bullet$ and $NO_2^\bullet$ radicals.

(6) The concerted pathway of the reaction DMS + *cis*-HOONO proceeds via the O−O bond cleavage barrier of 6.1 (6.3) kcal/mol at the **TS1(O−O activ.)** transition state, and leads exclusively to DMSO and HONO.

Acknowledgment. We thank the Cherry L. Emerson Center of Emory University for the use of its resources, which are in part supported by a National Science Foundation Grant (CHE-0079627) and an IBM Shared University Research Award. C.L.H. thanks the National Science Foundation Grant (CHE-0236686) for support.

Supporting Information Available: Cartesian coordinates of all calculated reactants, intermediates, transition states, and products of the reaction 1, (2) and (3) (**Table S1**), and their total energies (**Table S2**). The Mulliken charges (**Table S3**) and the calculated Δ*G*(solvation) values at the PCM level for all the reactants, intermediates, transition states, and products of the reaction 1 and (2). This material is available free of charge via the Internet at http://pubs.acs.org.

References and Notes

(1) (a) Nauser, T.; Koppenol, W. H. *J. Phys. Chem.* A **2002**, *106*, 4084, and references therein. (b) Goldstein, S.; Czapski, G. *Free Radical Biol. Med.* **1995**, *19*, 505, and references therein. (c) Huie, R. E.; Padmaja, S. *Free Radical Res. Commun.* **1993**, *18*, 195. (d) Beckman, J. S. The Physiological and Pathophysiological Chemistry of Nitric Oxide. In *Nitric*

Oxide: Principles and Actions; Lancaster, J., Ed.; Academic Press: San Diego, CA **1996**; p 1.

(2) (a) Goldstein, S.; Czapski, G.; Lind, J.; Merenyi, G. *Chem. Res. Toxicol*. **2001**, *14*, 657. (b) Edwards, J. O.; Plumb, R. C. *Prog. Inorg. Chem.* **1994**, *41*, 599. (c) Koppenol, W. H. *Met. Ions Biol. Syst.* **1999**, *36*, 597. (d) Pryor, W. A.; Squadrito, G. L. *Am. J. Physiol.* **1995**, *268*, L699, and references therein. (e) Merenyi, G.; Lind, J.; Goldstein, S.; Czapski, G. *J. Phys. Chem. A* **1999**, *103*, 5685.

(3) Kissner, R.; Koppenol, W. H. *J. Am. Chem. Soc.* **2002**, *124*, 234, and references therein.

(4) Pryor, W. A.; Gueto, R.; Jin, X.; Koppenol, W. H.; Ngu-Schwemlein, M.; Squadrito, G. L.; Uppu, P. L.; Uppu, R. M. *Free Radical Biol. Med.* **1995**, *18*, 75.

(5) (a) Beckman, J. S.; Beckman, T. W.; Chen, J.; Marshal, P. A.; Freeman, B. A. *Proc. Natl. Acad. Sci. U.S.A.* **1990**, *87*, 1620. (b) Coddington, J. W.; Hurst, J. K.; Lymar, S. V. *J. Am. Chem. Soc.* **1999**, *121*, 2438. (c) Richeson, C. E.; Mulder, P.; Bowry, V. W.; Ingold, K. U. *J. Am. Chem. Soc.* **1998**, *120*, 7211, and references therein. (d) Merenyi, G.; Lind, J.; Goldstein, S.; Czapski, G. *Chem. Res. Toxicol*. **1998**, *11*, 712.

(6) Rosen, G. M.; Freeman, B. A. *Proc. Natl. Acad. Sci. U.S.A.* **1984**, *81*, 7269.

(7) Marla, S. S.; Lee, J.; Groves, J. T. *Proc. Natl. Acad. Sci. U.S.A.* **1997**, *94*, 14243.

(8) Denicola, A.; Souza, J. M.; Radi, R. *Proc. Natl. Acad. Sci. U.S.A.* **1998**, *95*, 3566.

(9) Rachmilewitz, D.; Stamler, J. S.; Karmeli, F.; Mullins, M. E.; Singel, D. J.; Loscalzo, J.; Xavier, R. J.; Podolsky, D. K. *Gastroenterology* **1993**, *105*, 1681.

(10) Squadrito, G. L.; Jin. X.; Pryor, W. A. *Arch. Biochem. Biophys.* **1995**, *322*, 53.

(11) Lee, J.; Hunt, J. A.; Groves, J. T. *J. Am. Chem. Soc.* **1998**, *120*, 6053.

(12) Crow, J. P.; Beckman, J. S.; McCord, J. M. *Biochemistry* **1995**, *43*, 3544.

(13) Gatti, R. M.; Radi, R.; Augusto, O. *FEBS Lett.* **1994**, *348*, 287

(14) Szabo, C.; Ohshima, H. *Nitric Oxide: Biol. Chem.* **1997**, *1*, 373.

(15) (a) Halliwell, B.; Zhao, K.; Whiteman, M. *Free Radical Res.* **1999**, *31*, 651. (b) Pfeiffer, S.; Mayer, B.; Hemmens, B. *Angew. Chem., Int. Ed.* **1999**, *38*, 1715. (c) See ref 2c. (d) Groves, J. T. *Curr. Opin. Chem. Biol.* **1999**, *3*, 226. (e) Hurst, J. K.; Lymar, S. V. *Acc. Chem. Res.* **1999**, *32*, 520. (f) Trujillo, M.; Navillat, M.; Alvarez, M. N.; Peluffo, P.; Radi, R. *Analysis* **2000**, *28*, 518. (g) Radi, R.; Peluffo, P.; Alvarez, M. N.; Naviliat, M.; Cayota, A. *Free Radical Biol. Med.* **2001**, *30*, 463. (h) See ref 2d.

(16) (a) See refs 15f and 15 g, as well as: Radi, R. *Chem. Res. Toxicol.* **1998**, *11*, 720.

(17) (a) Stern, M. K.; Jensen, M. P.; Kramer, K. *J. Am. Chem. Soc.* **1996**, *118*, 8735. (b) Crow, J. P. *Arch. Biochem. Biophys.* **1999**, *371*, 41. (c) Lee, J.; Hunt, J. A.; Groves, J. T. *Bioorg. Med. Chem. Lett.* **1997**, *7*, 2913. (d) Hunt, J. A.; Lee, J.; Groves, J. T. *Chem. Biol.* **1997**, *4*, 845. (e) Crow, J. P. *Free Radical Biol. Med.* **2000**, *28*, 1487. (f) Balavoine, G. G. A.; Geletii, Yu. V.; Bejan, D. *Nitric Oxide: Biol. and Chem.* **1997**, *1*, 507. (g) Shimanovich, R.; Hannah, S.; Lynch, V.; Gerasimchuk, N.; Mody, T. D.; Magda, D.; Sessler, J.; Groves, J. T. *J. Am. Chem. Soc.* **2001**, *123*, 3613. (h) Zhang, X.; Busch, D. H. *J. Am. Chem. Soc.* **2000**, *122*, 1229. (i) Salvemini, D.; Wang, Z. Q.; Stern, M.; Currie, M. G.; Misko, T. *Proc. Natl. Acad. Sci. U.S.A.* **1998**, *95*, 2659. (j) Groves, J. T.; Marla, S. S. *J. Am. Chem. Soc*. **1995**, *117*, 9578.

(18) See: Jensen, M. P.; Riley, D. P. *Inorg. Chem*. **2002**, *41*, 4788, and references therein

(19) (a) Floris, R.; Piersma, S. R.; Yang, G.; Jones, P.; Wever, R. *Eur. J. Biochem.* **1993**, *215*, 767. (b) Kondo, H.; Takahashi, M.; Niki, E. *FEBS Lett.* **1997**, *413*, 236. (c) Exner, M.; Herold, S. *Chem. Res. Toxicol.* **2000**, *13*, 287. (d) Minetti, M.; Scorza, G.; Pietraforte, D. *Biochemistry* **1999**, *38*, 2078. (e) Herold, S.; Matsui, T.; Watanabe, Y. *J. Am. Chem. Soc*. **2001**, *123*, 4085. (f) Bourassa, J. L.; Ives, E. P.; Marqueling, A. L.; Shimanovich, R.; Groves, J. T. *J. Am. Chem. Soc*. **2001**, *123*, 5142.

(20) *Selenium in Biology and Human Health*; Burk, R. F., Ed.; Springer-Verlag: New York, 1994, and references therein.

(21) (a) Mugesh, G.; Singh, H. B. *Chem. Soc. Rev.* **2000**, *29*, 347. (b) Mugesh, G.; Panda, A.; Singh, H. B.; Punekar, N. S.; Butcher, R. J. *J. Am. Chem. Soc*. **2001**, *123*, 839. (c) Mugesh, G.; du Mont, W. W.; Sies, H. *Chem. Rev*. **2001**, *101*, 2125, and references therein. (d) Briviba, K.; Roussyn, I.; Sharov, V. S.; Sies, H. *Biochem. J.* **1996**, *319*, 13.

(22) (a) Sies, H.; Masumoto, H. *Adv. Pharmacol*. **1997**, *38*, 2229 and references therein. (b) Masumoto, H.; Sies, H. *Chem Res. Toxicol.* **1996**, *9*, 262. (c) Masumoto, H.; Kissner, R.; Koppenol, W. H.; Sies, H. *FEBS Lett.* **1996**, *398*, 179

(23) (a) Perrin, D.; Koppenel, W. H. *Arch. Biochem. Biophys.* **2000**, *377*, 266. (b) Pryor, W. A.; Jin. X.; Squadrito, G. J. *Proc. Natl. Acad. Sci. U.S.A.* **1994**, *91*, 11173.

(24) Jensen, J. L.; Miller, B. L.; Zhang, X.; Hug, G. L.; Schoeneich, C. *J. Am. Chem. Soc*. **1997**, *119*, 4749.

(25) (a) Goldstein, S.; Squadrito, G. L.; Pryor, W. A.; Czapski, G. *Free Radical Biol. Med.* **1996**, *21*, 965. (b) Koppenel, W. H.; Kissner, R. *Chem. Res. Toxicol.* **1998**, *11*, 87.

(26) Tsai, H. H.; Hamilton, T. P.; Tsai, J. H. M.; Van der Woerd, M.; Harrison, J. G.; Jablonsky, M. J.; Beckman, J. S.; Koppenol, W. H. *J. Phys. Chem.* **1996**, *100*, 15087.

(27) Koppenol, W. H.; Moreno, J. J.; Pryor, W. A.; Ischiropoulos, H.; Beckman, J. S. *Chem. Res. Toxicol.* **1992**, *5*, 834.

(28) Goss, S. P. A.; Singh, R. J.; Hogg, N.; Kalyanaraman, B. *Free Rad. Res*. **1999**, *31*, 597.

(29) (a) Miertus, S.; Scrocco, E.; Tomasi, J. *Chem. Phys.* **1981,** *55*, 117. (b) Miertus, S.; Tomasi, J. *Chem. Phys.* **1982,** *65*, 239. (c) Cossi, M.; Barone, V.; Cammi, R.; Tomasi, J. *Chem. Phys. Lett.* **1996**, *255*, 327. (d) Cances, M. T.; Mennucci, V.; Tomasi, J. *J. Chem. Phys.* **1997**, *107*, 3032. (e) Barone, V.; Cossi, M.; Tomasi, J. *J. Comput. Chem.* **1998**, *19*, 404.

(30) (a) Houk, K. N.; Condroski, K. R.; Pryor, W. A. *J. Am. Chem. Soc*. **1996**, *118*, 13002. (b) Houk, K. N.; Liu, J.; DeMello, N. C.; Condorski, K. R. *J. Am. Chem. Soc*. **1997**, *119*, 10147. (c) Yang, D.; Tang, Y, C.; Chen, J.; Wang, X. C.; Bartberger, M. D.; Houk, K. N.; Olson, L. *J. Am. Chem. Soc*. **1999**, *122*, 11976.

(31) Musaev, D. G.; Hirao, K. *J. Phys. Chem. A* **2003**, *107*, 1563.

(32) Bach, R. D.; Gluhkovtsev, M. N.; Canepa, C. *J. Am. Chem. Soc*. **1998**, *120*, 775.

(33) Shustov, G. V.; Spinney, R.; Rauk, A. *J. Am. Chem. Soc*. **2000**, *122*, 1191.

(34) Musaev, D. G.; Geletii, Yu. V.; Hill, C. L.; Hirao, K. *J. Am. Chem. Soc.* **2003**, *125*, 3877.

(35) Frisch, M. J.; Trucks, G. W.; Schlegel, H. B.; Scuseria, G. E.; Robb, M. A.; Cheeseman, J. R.; Zakrzewski, V. G.; Montgomery, J. A., Jr.; Stratmann, R. E.; Burant, J. C.; Dapprich, S.; Millam, J. M.; Daniels, A. D.; Kudin, K. N.; Strain, M. C.; Farkas, O.; Tomasi, J.; Barone, V.; Cossi, M.; Cammi, R.; Mennucci, B.; Pomelli, C.; Adamo, C.; Clifford, S.; Ochterski, J.; Petersson, G. A.; Ayala, P. Y.; Cui, Q.; Morokuma, K.; Malick, D. K.; Rabuck, A. D.; Raghavachari, K.; Foresman, J. B.; Cioslowski, J.; Ortiz, J. V.; Baboul, A. G.; Stefanov, B. B.; Liu, G.; Liashenko, A.; Piskorz, P.; Komaromi, I.; Gomperts, R.; Martin, R. L.; Fox, D. J.; Keith, T.; Al-Laham, M. A.; Peng, C. Y.; Nanayakkara, A.; Gonzalez, C.; Challacombe, M.; Gill, P. M. W.; Johnson, B.; Chen, W.; Wong, M. W.; Andres, J. L.; Gonzalez, C.; Head-Gordon, M.; Replogle, E. S.; Pople, J. A. *Gaussian 98*, Revision A.7; Gaussian, Inc.: Pittsburgh, PA, 1998.

(36) (a) Becke, A. D. *Phys. Rev. A* **1988**, *38*, 3098. (b) Lee, C.; Yang, W.; Parr, R. G. *Phys. Rev. B* **1988**, *37*, 785. (c) Becke, A. D. *J. Chem. Phys.* **1993**, *98*, 5648.

(37) Tsai, J. H. M.; Harrison, J. G.; Martin, J. C.; Hamilton, T. P.; Van der Woerd, M.; Jablonsky, M. J.; Beckman, J. S. *J. Am. Chem. Soc*. **1994**, *116*, 4115.

(38) McKee, M. L. *J. Am. Chem. Soc*. **1995**, *117*, 1629.

(39) Lynch, B. J.; Fast, P. L.; Harris, M.; Truhlar, D. G. J. *Chem. Phys.* A **2000,** *104*, 4811.

(40) (a) Liang, B.; Andrews, L. *J. Am. Chem. Soc*. **2001**, *123*, 9848, and references therein. (b) Krauss, M. *Chem. Phys. Lett.* **1994**, *222*, 513.

(41) Fan, Y. B.; Ding, Z. B.; Wang, Q. R.; Tao, F. G. *Chem. Phys. Lett.* **2000**, *328*, 39, and references therein.

(42) Nakanishi, W.; Hayashi, S. *J. Chem. Phys.* **1999**, *103*, 6074, and references therein.

(43) (a) Gonzalez, C.; Schlegel, H. B. *J. Chem. Phys*. **1989**, *90*, 2154. (b) Gonzalez, C.; Schlegel, H. B. *J. Phys. Chem.* **1990**, *94*, 5523.

(44) *CRC Handbook of Chemistry and Physics*, 72nd ed.; Lide, D. R., Ed.; CRC Press: Boca Raton-Ann Arbor-Boston, 1991−1992.

(45) The exothermicity of $ONOO^-$ isomerization in water was estimated to be $\Delta G^\circ = -(40.5-43.1)$ kcal/mol on the basis of the values of $\Delta_f G^\circ(ONOO^-) = -14$ [Nauser, T.; Koppenol, W. H. *Chem. Res. Toxicol.* **2001**, *14*, 348] or 16.6[5d] kcal/mol, and $\Delta_f G^\circ(NO_3^-) = -26.5$ kcal/mol[47] in water.

(46) McGrath, M. P.; Rowland, F. S. *J. Chem. Phys.* **1994**, *98*, 1061, and references therein

(47) Bartberger, M. D.; Olson, L. P.; Houk, K. N. *Chem Res. Toxicol.* **1998**, *11*, 710, and references therein.

(48) (a) Sumathi, R.; Peyerimhoff, S. D. *J. Chem. Phys.* **1997**, *107*, 1872, (b) Bach, R. D.; Ayala, P. Y.; Schelegel, H. B. *J. Am. Chem. Soc.* **1996**, *118*, 12758.

(49) Pfeiffer, S.; Mayer, B.; Janoschek, R. *J. Mol. Struct. (THEOCHEM)* **2003**, *623*, 95.

(50) (a) Merenyi, G.; Lind, J.; Engman, L. *J. Phys. Chem.* **1996**, *100*, 8875. (b) Schoneich, C.; Aced, A.; Asmus, K. D. J. *Am. Chem. Soc.* **1993**, *115*, 11376. (c) Miller, B.; Williams, T. D.; Schoneich, C. *J. Am. Chem. Soc.* **1996**, *118*, 11014, and references therein.

(51) Peroxynitrite is used to refer to the peroxynitrite anion, $O{=}NOO^-$, and peroxynitrous acid, ONOOH, unless otherwise indicated. The IUPAC recommended names are oxoperoxonitrate (−1) and hydrogen oxoperoxonitrate, respectively. The abbreviation PN is used in this paper to refer to the peroxynitrite anion.